

The effect of propagation saw test geometries on critical cut length

Bastian Bergfeld^{1*}, Karl W. Birkeland², Valentin Adam^{1,3}, Philipp L. Rosendahl³, and Alec van Herwijnen¹

¹ WSL Institute for Snow and Avalanche Research SLF, Davos, Switzerland

² Birkeland Snow and Avalanche Scientific, Bozeman, Montana

³ Institute of Structural Mechanics and Design, Technical University of Darmstadt, Darmstadt, Germany

Correspondence to: Bastian Bergfeld (bastian.bergfeld@slf.ch)

Abstract:

For a slab avalanche to release, a crack in a weak snow layer beneath a cohesive snow slab has to initiate and propagate. Information on crack propagation is essential for assessing avalanche triggering potential. In the field, this information can be gathered with the Propagation Saw Test (PST), a field test that provides valuable data on crack propagation propensity. The first PSTs were performed about 20 years ago and standards have since been established. However, there are still differences in how the PST is performed. Standards in North America require the column ends to be cut vertically, whereas in Europe they are typically cut ~~at a normal angle~~normal to the slope. In this study, we investigate the effect of these different column geometries on the critical cut length. To this end, we conducted 27 pairs of PST experiments, each pair consisting of one PST with slope normal cut ends and one PST with vertical cut ends. Our experiments showed that PSTs with normal cut ends have up to 50% shorter critical cut lengths, and the difference predominantly depends on the slope angle and slab thickness. We developed two load-based models to convert critical cut lengths between the test geometries: (i) a uniform slab model that treats the slab as one uniform layer and (ii) a layered model that accounts for stratification. For validation, we compare these models with a modern fracture mechanical model. For the rather uniform slabs of our experiments, both load-based models were in excellent agreement with measured data. For slabs with an artificial layering, the uniform load-model predictions reveal deviations from the fracture mechanical model whereas the layered model was still in excellent agreement. This study reveals the influence that the geometry of field tests and the slope angle of the field site have on test results. It also shows that only accurately prepared field tests can be reliable and therefore meaningful. However, we provide models to correct for imprecise field test geometry effects on the critical cut length.

KEYWORDS: stability test, Propagation Saw Test, edge effect, failure initiation

1 Introduction

Accurate assessment of fracture initiation and crack propagation is essential to evaluate the potential for triggering avalanches (Schweizer et al., 2016). In this context, the Propagation Saw Test (PST) is a field test that provides valuable insight into the propensity of cracks to propagate (Gauthier and Jamieson, 2006b). In the past 20 years several studies investigated the influence of PST geometry. They aimed to provide recommendations for the PST column length (Bair et al., 2014) or looked into the effect of changing slab thicknesses (Simenhois and Birkeland, 2008). It was also reported that the critical cut length depends on whether the ends of the PSTs are cut slope-normally or vertically (Gaume et al., 2017). Although PSTs have been used for approximately 20 years and utilized in various studies (Bair et al., 2013;

37 Bergfeld et al., 2022; Bergfeld et al., 2021; Birkeland et al., 2019; Gauthier and Jamieson, 2008b), the lack of widely
38 accepted standards hinders its consistent and reproducible application across locations and practitioners. Standards in
39 North America require the PST column ends to be cut vertically (CAA, 2016; Greene et al., 2022), whereas in Europe
40 they are typically cut at a normal to the slope (Sigrist and Schweizer, 2007; van Herwijnen et al., 2016).

41 This methodological difference could possibly explain why previous studies were not conclusive as to whether the crit-
42 ical cut length decreases (Gaume et al., 2017, slope normal cuts) or increases (Gauthier and Jamieson, 2008a; McClung,
43 2009, both slope vertical cuts) with increasing slope angle. In both, North America and Europe the weak layer is most
44 commonly cut upslope, but in rare cases, the weak layer is also cut downslope from the top. Gauthier and Jamieson
45 (2006a) investigated this difference experimentally and observed no significant dependence of critical cut length on cut-
46 ting direction. However, they also found that critical cut length does not depend on slope angle. Another contradictory
47 statement about the cut length to slope angle relationship. However, the geometric and/or methodological differences
48 (column geometry and cutting direction of PSTs) are likely to affect the results of PSTs (Gaume et al., 2017; Heierli et
49 al., 2008, Supplement Figure S3). Our study aims to investigate the effect of different column geometries and cutting
50 directions on the critical cut length, a major structural property. To achieve this, we conducted a series of side-by-side
51 PST experiments with normal and vertical ends. In addition, we also investigated the influence of cutting direction
52 (upslope or downslope).

53

54 The purpose of these experiments was to demonstrate the influence of PST column geometry and cutting direction on the
55 critical cut length. We also explain where these differences come from and how the stratification of the snowpack influ-
56 ence these geometric effects. To this end, we developed a uniform- and layered load-based models to convert between
57 PST geometries. In addition, the developed conversion models were validated against a modern fracture mechanics model
58 (Rosendahl and Weissgraeber, 2020; Weißgraeber and Rosendahl, 2023).

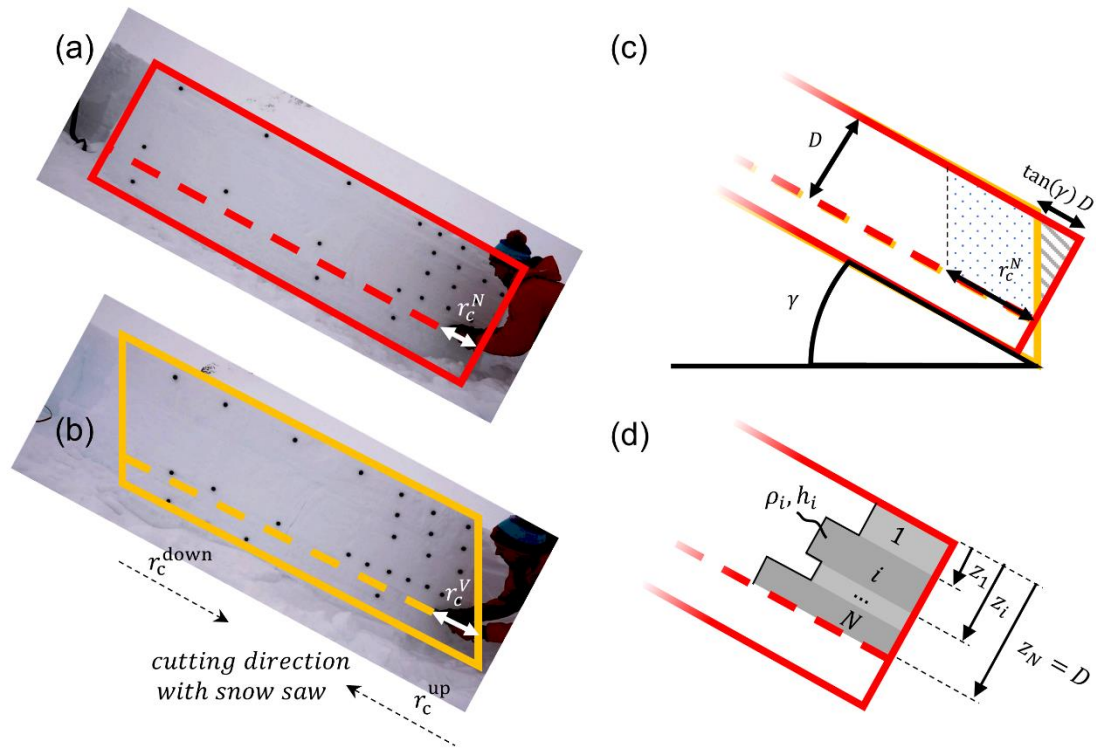
59 **2 Methods**

60 **Field Experiments**

61 In January and March 2021, we performed field experiments above Davos in the Eastern Swiss Alps, and in Montana,
62 United States. All field sites were around 2400 m.a.s.l. and PSTs resulted in all possible propagation outcomes (slab
63 fracture, crack arrest and full propagation). In Davos, we tested a weak layer consisting of surface hoar (grain size: 2-4
64 mm), while in Montana the weak layer consisted of depth hoar (grain size: 1-4 mm) (Fierz et al., 2008). Slab thickness
65 ranged from 52 to 96 cm.

66

67 In total 27 pairs of PSTs were performed, with each pair consisting of one test using slope normal ends (results with
68 superscript X^N, Figure 1Figure 1a) and the other with vertical ends (superscript X^V, Figure 1Figure 1b). For three pairs,
69 hence for six PSTs, we performed additional PSTs in which the weak layer was cut in downslope direction immediately
70 next to the PST cut in the upslope direction (r_c^{up} and r_c^{down} in Figure 1Figure 1b).



94

95

96 **Figure 1:** (a) PST with normal ends and a critical cut length r_c^N . The red outline indicates the PST geometry. The dashed line indicates the height of the weak layer. (b) PST with vertical ends and a critical cut length r_c^V . **Additionally, the different cutting directions r_c^{up} and r_c^{down} are indicated. The two cutting directions were used in both PST geometries.** (c) Difference in PST geometry **at the downslope end of a PST**. The main difference is the additional slab load for the slope normal geometry shown by the grey triangle. H^V is the vertical measured slab thickness and γ the slope angle. (d) In the layered load conversion model, each slab layer i contributes according to their density ρ_i , layer thickness h_i and depth in the slab z_i .

102 For all PSTs, we recorded the critical cut length as r_c^N for PSTs with normal ends, and r_c^V for vertical ends. We then
 103 compute the ratio of both cut lengths r_c^V / r_c^N . To investigate the effect of cutting directions, we used the ratio r_c^{up} / r_c^{down} ,
 104 where r_c^{up} and r_c^{down} indicate whether the critical cut length was taken from upslope or downslope cutting of the weak
 105 layer, respectively (Figure 1). **Note that the ratio of the cutting direction was determined separately for the**
 106 **different PST geometries.**

107

108 Conversion Models

109 Mechanically, a PST can be modelled as a cantilever beam. The cantilever (unsupported part of the slab) is loaded by the
 110 gravitational body forces, hence its own mass. This loading has to be carried through a combination of reaction forces,
 111 shear forces, and bending moments inside the slab, which all work together to resist the load and maintain the slab's
 112 structural integrity. The stress transmitted from the slab to the foundation is known as bearing stress or contact stress. As
 113 the foundation is provided by the intact weak layer, the contact stress is transmitted right ahead of the saw cut.
 114 Simplified, the contact stress is related to the reaction force of the weak layer which supports the cantilever. For a
 115 levelled cantilever beam, the vertical reaction force R at the bedding is equal to the total load of the unsupported part of
 116 the slab: $R = m g$, where m is the total mass of the slab above the saw cut and g is the gravitational acceleration. The

Form

117 maximum load; a weak layer can support before fracture is reached at the critical cut length. Hence, also R is at a maxi-
 118 imum at the critical cut length (R_{max}). In our load models, we assume that R_{max} is specific to a weak layer, which enables
 119 us to state that: $R_{max} = R_{max}^V = R_{max}^N$, where R_{max}^V and R_{max}^N are the reaction forces at the critical cut length which
 120 bear the unsupported portion of the slab in the slope-vertical and slope-normal PST geometry, respectively. As the grav-
 121 itational acceleration is constant, we basically equal the masses of the unsupported slab of the two PST geometries are
 122 equal:

$$m^V = m^N \quad (1)$$

123 Note, that also the mass of the slab above the intact weak layer contributes to R_{max} , but sinceas these are additive terms
 124 which are independent of PST geometry, they cancel each other out in equation 1.

125
 126
 127 **Uniform Load Model (ULM).** If we consider a uniform slab and express the mass m through snowpack properties
 128 equation 1 reads tobecomes:

$$\rho b r_c^V D = \rho b r_c^N D + \frac{1}{2} \tan(\gamma) D D \rho b \quad (2)$$

129 where D is the slope normal measured slab thickness, γ the slope angle, b the PST column thickness and ρ the slab density
 130 (Figure 1Figure 1c). After rearranging, equation 2 results in the following model for the conversion of critical cut lengths
 131 (assumption of a uniform slab):

$$r_c^V = r_c^N + \frac{\tan(\gamma) D}{2} \quad (3)$$

132
 133 At this point we would like to point out that this relationship (Equation 3) was already suggested in the context of anticrack
 134 nucleation. However, the derivation was based purely on geometric considerations and no further verification was carried
 135 out (Heierli et al., 2008, Supplement Figure S3).

136
 137 **Layered Load Model (LLM).** The temporal sequence of weather conditions inevitably produces layered slabs in a nat-
 138 ural snowpack. The individual layers differ, among other parameters, in their layer thickness and density. A sloped PST
 139 with layered slab in slope normal geometry results in more (compared to the ULM) load above the saw cut if high density
 140 layers are close to the snow surface (grey triangle in (Figure 1Figure 1c and d). In addition to the slope angle γ , the extra
 141 load depends on the individual layer thickness h_i , density ρ_i , and on the relative depth z_i within the slab (Figure 1Figure
 142 1d). Conceptually, the layered load model is based on the same assumptions as the uniform load model. However, it
 143 considers the layering which makes the formulation to compute the additional load of PSTs with slope normal geometry
 144 more intricate:

$$r_c^V = \frac{\sum_{i=1}^N r_c^N h_i \rho_i + \frac{\tan(\gamma)}{2} h_i^2 \rho_i + \tan(\gamma) (z_N - z_i) h_i \rho_i}{\sum_{i=1}^N h_i \rho_i} \quad (4)$$

145
 146 Where N is the number of layers. Hence for $N = 1$, equation 4 simplifies to the ULM (equation 3). For a detailed derivation
 147 of the layered load model, see Appendix A.

148 149 **Layered Mechanical Model (LMM).**

150 For further verification of the load models, we use a closed-form analytical model for layered snowpacks (Weißgraeber
 151 and Rosendahl, 2023) that was recently validated with field data (Bergfeld et al., 2023), has been utilized. This model
 152 describes the slab as shear-deformable, layered beam, and allows cylindrical bending, while the weak layer is represented
 153 as a layer of smeared springs with a Young's and shear modulus. We used the model to determine the critical energy

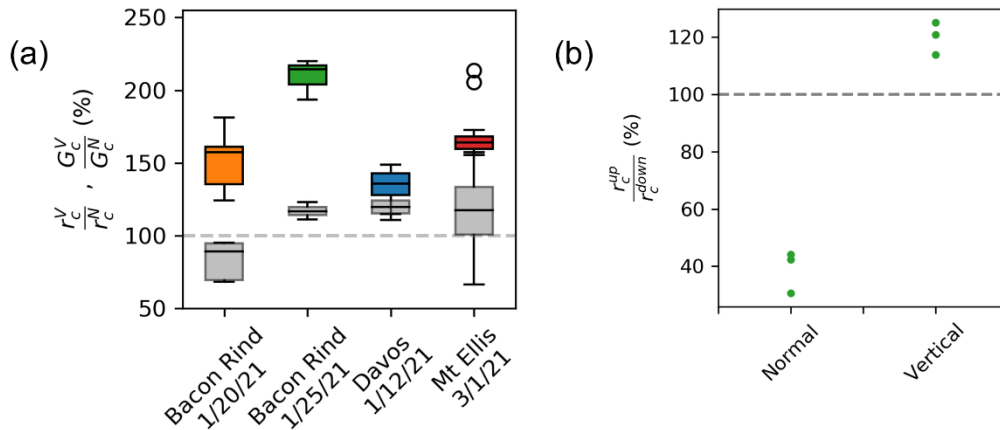
154 release rate G from the measured critical cut length, depending of the geometric configuration (G_c^N or G_c^V , respectively).
 155 This critical energy release rate, also called specific fracture energy, is a material property of the weak layer describing
 156 its resistance to crack growth, and it is hence a proxy for the fundamental physical process of crack growth in PSTs.
 157 Subsequently, we used the critical energy release rate determined from an experiment with slope normal beam ends to
 158 calculate back to the critical cut length of a vertically cut PST. This model is therefore also suitable to convert a critical
 159 cut length measured in one PST configuration to another. Compared to the ULM (Equation 3) and the LLM (Equation 4),
 160 the LMM requires many more snowpack properties. However, it represents the specific snowpack layering of a PST and
 161 its influence on the critical cut length in much more detail, as it takes into account the full deformation behaviour of the
 162 slab and weak layer system. We therefore used the LMM to verify the influence of an asymmetrically layered slab on our
 163 load-based models (ULM, LLM).

164 **Results**

165 In total we performed 66 PSTs at four different field sites. 54 PSTs aimed to investigate the effect of PST geometry
 166 (Appendix, Table C1), therefore the dataset include 27 pairs of PSTs and each pair consists of one PST with slope normal
 167 and one with vertical PST beam ends. The remaining 12 PSTs were performed to investigate the difference between
 168 upslope- and downslope cutting of a PST (Appendix, Table C2).

169 **Normal vs. vertical PST ends**

170 Critical cut lengths were measured between 14 and 70 cm. Overall, r_c^V was systematically larger than r_c^N , on average
 171 almost 50 % (colored boxes in Figure 2a).



172
 173 **Figure 2: (a) Ratio of critical cut lengths shown as boxplots for the different field days (colored). Ratio of the critical energy**
 174 **release rates computed with the mechanical model using the critical cut lengths of the experiments (grey). Boxes represent the**
 175 **inter-quartile range with the middle line representing the median value. (b) Ratio of critical cut length from PSTs with**
 176 **downslope and upslope cuts. Results are shown for PSTs with normal and vertical PST ends. Both: The dashed line represents**
 177 **a ratio of 1.**

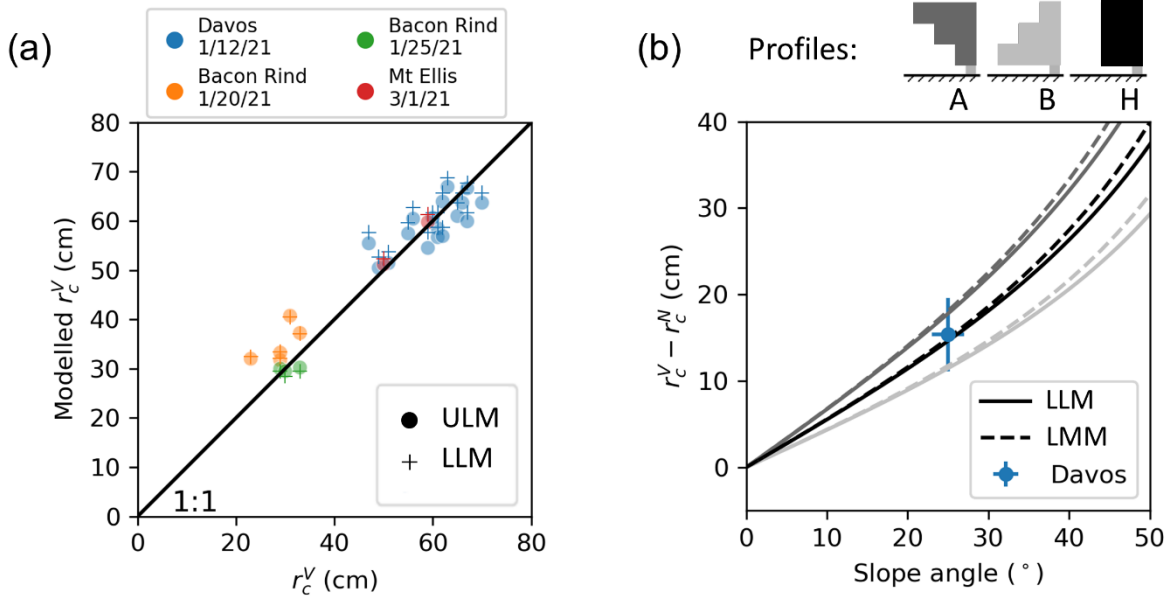
178 Differences in snowpack conditions at the various field sites resulted in different deviations between PST geometries.
 179 Median ratios ranged from 136 % to 214 % (Figure 2a, horizontal lines in the colored boxes).

180 **Upslope vs. Downslope cutting**

181 Beside PST geometry, the cutting direction also affects the critical cut length. For PSTs with normal ends, r_c^{up} was about
 182 40% of r_c^{down} (Figure 2b, left), while for vertical PST ends r_c^{up} was about 20% longer than r_c^{down} (Figure 2b, right).
 183 Again, these rather large differences can be explained by slab loading and slab mechanics as will be detailed in the dis-
 184 cussions section.

185 **Models**

186 With Equations (3) and (4) we provide a **uniform load model** and a **layered load model**, respectively. The models allow
 187 us to convert critical cut lengths between the different PST geometries. Our experiments show very good agreement with
 188 both the uniform-load model (Figure 3a, dots) and the layered load model (Figure 3a, crosses). The RMSE between the
 189 measured critical cut lengths in vertical geometry r_c^V and the modelled counterpart is 4.4 cm for the uniform load model
 190 and 4.6 cm for the layered load model.



191
 192 **Figure 3:** (a) Modelled critical cut lengths for upslope cuts with vertical PST geometry r_c^V with the corresponding measured
 193 values, dots represent the uniform load model (ULM, Equation 2) and pluses the layered load model (LLD, Equation 3). Dif-
 194 ferent colors indicate the different field days. The black line is the 1:1 line and indicates a perfect model. (b) Modelled differ-
 195 ences in critical cut lengths with slope angle. The blue dot represents the mean and uncertainty of the measurements in Davos,
 196 as this field day served to define the artificial profiles by matching the mean density. The solid lines are the layered load model
 197 and the dashed lines result from the layered mechanical model (LMM). The grey shades indicate different slab profiles given
 198 at the top of the figure.

199 Using the **layered mechanical model** to analyse the global energy balance at the onset of crack growth, we derived
 200 critical energy release rates from the experimental data. The model considers the layering and geometrical configuration
 201 of a PST experiment to determine the critical energy release rate at the critical cut length, i.e., the specific fracture energy.
 202 Unlike the critical cut length, the critical energy release rate is a material property of the weak layer and should thus not
 203 depend on test geometry. In fact, the determined critical energy release rates, measured in the different PST configurations
 204 (vertical or normal beam ends), differed by a maximum of 20% (Figure 2a, grey boxes), whereas the deviations of the
 205 critical cut length were up to six times larger (Figure 2a, coloured boxes).
 206

207 Our **uniform load model** considers a homogeneous slab and gives a tangential slope dependence (see Equation 3 and
208 black solid line in Figure 3b). For comparison, the **layered load model** and the **layered mechanical model** were evaluated
209 for many different slope angles (Figure 3b, solid and dashed lines, respectively) and 3 different generic slab configurations
210 (Figure 3b, top). In profile H the mean slab density matched the observed snow cover at our experiments in Davos. The
211 direct comparison for the artificial profile H shows a very good agreement between the load models and the mechanical
212 model (compare black solid line and black dashed line in Figure 3b). Note that for profile H the two load models are
213 equal. The deviations of the critical cut lengths ($r_c^V - r_c^N$) measured in Davos can be reproduced very accurately with all
214 models (Figure 3b, black lines and blue dot). In the asymmetric profiles A and B, additional artificial layers with the
215 minimum and maximum density of the Davos snow profile were inserted. For these highly asymmetric slabs (grey lines
216 in Figure 3) there are deviations between the models. Of course, the uniform model cannot represent any differences
217 induced by the layering. However, the layered load model and the mechanical model show good agreement over the entire
218 angle range, whereby the deviations slightly increase with increasing slope angles.

219 **Discussion**

220 **Normal vs. vertical PST ends**

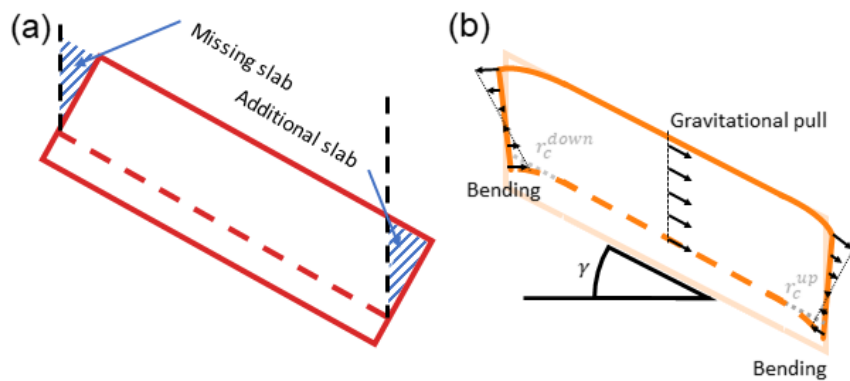
221 PSTs with slope-normal and vertical ends showed large differences in the measured critical cut length. These differences
222 can be explained with the different PST geometries and the corresponding slab-induced loading of the weak layer. We
223 assume that PST beams were long enough, so that the tail end of the PST beam remains mechanically unchanged when
224 the saw cut is increased and is therefore not relevant (Bair et al., 2014). The constellation is as shown schematically in
225 Figure 1c. Even with no saw cut, the slope normal PST geometry already has an "unsupported" portion of the slab above
226 the weak layer (Figure 4a, blue area at the right beam end). This additional load, in normal geometry, generates higher
227 stresses in the weak layer (and higher energy release rate), leading to shorter critical cut lengths. The shorter critical cut
228 lengths can therefore easily be attributed to this additional load. However, the extent of the difference depends on snow-
229 pack properties (e.g. slab thickness, density layering) and slope angle.

230
231 This emphasizes that a measured critical cut length can only be interpreted for stability assessment if the applied geometric
232 PST configuration (including slope angle) is considered. In other words, our data show that two equal snowpacks, which
233 should exhibit a similar crack propagation propensity, likely result in completely different critical cut lengths depending
234 on how the PST beam ends were cut and on which slope angle the PST was performed. To ensure comparability of
235 measured critical cut lengths, it is thus imperative to account for the geometrical configuration and snowpack layering,
236 using the models presented.

237 **Upslope vs. Downslope cutting**

238 When cutting upslope, there is an additional part of the slab that induces an extra load on the weak layer in the slope
239 normal configuration (Figure 4a, blue area at the right beam end). When cutting from the top, however, a part of the slab
240 is missing, and there is less load (Figure 4a, blue area at the left beam end). The critical cut length of the upslope cut is
241 thus much shorter, in our experiments about 60% shorter (left side in Figure 2b).
242

243 In the vertical configuration, on the other hand, the load over the saw cut is always the same, independent of the cutting
 244 direction. The observed differences, however, come from the differences in shear stress at the crack tip. Indeed, at the
 245 weak layer, there are two shear stress components: (i) shear stress from the slope parallel gravitational pull on the slab
 246 (Figure 4b, arrows in the middle), and (ii) bending induced shear stresses (Figure 4b, arrows at the left and right beam
 247 end). The slope parallel gravitational pull is always in the same direction (downslope). The bending induced shear stresses
 248 at the height of the weak layer, on the other hand, are always in the cut direction. When cutting the weak layer from the
 249 bottom upwards, both contributions thus have an opposite effect and partially cancel each other out, while when cutting
 250 from the top, both shear stresses have the same sign and add up. This results in longer critical cut lengths when sawing
 251 upslope in vertical PSTs. In our measurements, these were 20% longer (right side in Figure 2b).
 252



253
 254 **Figure 4:** (a) Schematic representation of a PST with normal ends and without a saw cut. The blue marked areas, at the right
 255 and left of the PST beam, indicate the additional and missing slab load, respectively, relative to vertical ends (black dashed
 256 lines). (b) PST with vertical ends and critical cut lengths r_c^{up} and r_c^{down} for upslope and downslope cutting, respectively. At
 257 both PST beam ends the saw cut leads to bending, which results in a stress profile across the slab thickness (black arrows). In
 258 the middle part of the PST, the black arrows represent stress in the slab due to the slope parallel gravitational pull. γ is the
 259 slope angle.

260
 261 **Models**

262 Overall, the load models effectively explained our field results. (Figure 3a). If the RMSE of the uniform load- and layered
 263 load model is compared, the uniform load model performs slightly better than the layered load model. However, since
 264 our snowpack profiles show relatively homogeneous slabs without pronounced asymmetry (see Appendix D), we would
 265 not attach any significance to this minor difference, especially for inhomogeneous and asymmetrical slabs. We believe
 266 the layered load model is more accurate. This becomes clear in Figure 3b. Profiles A and B have a density gradient
 267 within the slab (asymmetry). Deviations between the uniform and the layered load model seem plausible as higher density
 268 layers which are close to the snow surface contribute more to the additional load present in slope normal PSTs (blue
 269 hashed in Figure 4a) than if they are deeper in the snowpack. The difference in critical cut lengths is expected to be larger
 270 (profile A) or smaller (profile B) than predicted by the uniform load model.

271
 272 Beside the overall good conversion performance of the models, a systematic offset for PSTs from 20 January 2021 seem
 273 to be present (orange dots in Figure 3). We suspect that in these PSTs the beam length was too short, the ratio between
 274 slab thickness and beam length was only about 0.5 and the cut length to beam length ratio was 0.25. It is therefore very

275 likely that the geometric difference at the tail end of the beam was also relevant (Bair et al., 2014). However, this is not
276 considered in the models. Overall, our results thus show that the PST geometry plays an important role in the measured
277 critical cut length, and this is mostly driven by differences in load from the slab.

278

279 **Model application and limitation:**

280 PST datasets with different PST configurations can be homogenised using our models. This will increase the compara-
281 bility and ultimately the scientific utility of these datasets. In addition, it is often the case that the PST ends are cut
282 imprecisely (not perfectly vertical or slope normal) on inclined terrain. The angle of the free edge can easily be determined
283 from photos of the test, and a correction can then be applied using one of the load models with minor modifications
284 (Appendix B). The scatter of the experimentally determined critical cut lengths should thus be reduced.

285 Beside applications, shortcomings of the suggested load models are evident. ~~The suggested load models rely on Equa-
286 tion 1, rearranged it reads to: $\tau_{\epsilon}^V \sigma^V \propto \tau_{\epsilon}^N \sigma^N$. Using equation A2 (Appendix A) the unit on both sides of the relation is
287 $\frac{J}{m^2}$, an energy per unit area. The interpretation of Equation 1 is similar to equating both PST configurations (vertical
288 and normal cut ends) by the specific fracture energy of the weak layer, which is a reasonable approach followed by the
289 layered mechanical model. However, equation 1 remains freely chosen because it is not the fracture energy that is com-
290 puted by $\tau_{\epsilon}^X \sigma^X$. Although, our experimental results show that the relationship is sufficiently accurate for the conver-
291 sion of PST geometries, additional changes, beyond the PST geometry, are directly affecting model performance, so the
292 relationship may no longer be sufficient. Imagine additional terms from factors A and contributions B in Equation 1:~~

$$293 \quad A(\gamma, H^N, \dots) m^V + B(\gamma, H^N, \dots) \propto A(\tilde{\gamma}, \tilde{H}^N, \dots) m^N + B(\tilde{\gamma}, \tilde{H}^N, \dots)$$

294 Both can have functional relationships on properties such as slope angle ($\gamma, \tilde{\gamma}$) and slab thickness (H^N, \tilde{H}^N).

295 As long as such properties remain unchanged ($\gamma = \tilde{\gamma}, H^N = \tilde{H}^N$), the additional terms cancel each other out and our load
296 models are applicable.

297 However, if the critical cut length measured at a certain slope angle and snow cover has to be transferred to a different
298 situation, the applicability of our models still needs to be confirmed with more experimental work. If necessary, the
299 functional relationships A and B will probably have to be identified and added. A more generally valid conversion for
300 critical cut lengths would be of great practical benefit as it allows to extrapolate measured point information on crack
301 propagation propensity to other slope areas where experimental work is not possible.

302 **Conclusion and Outlook**

303 This work has shown that the result of a PST, i.e., the measured critical cut length, is strongly influenced by the test
304 geometry and cutting direction. PSTs with slope normal beam ends systematically produce shorter critical cut lengths
305 (48% on average). It also makes a significant difference whether the saw cut in a PST is made in the upslope or downslope
306 direction (deviations up to 60%). Both deviations can be explained mechanically and are largely controlled by the differ-
307 ence in slab induced loads. Based on the slab load, a load model was derived for uniform, as well as for layered slabs.
308 Both models agree well with the experimental results. The comparison with a more sophisticated validated fracture me-
309 chanical model shows good agreement between all models as long as the slab is largely homogeneous. For layered slabs,
310 the uniform load model shows greater deviations. The layered load model, on the other hand, shows only minor deviations.
311 This demonstrates that the fracture mechanical model (LMM) is also largely load-driven in this specific application.

312 Overall, our results show that the interpretation of measured critical cut length in a PST is not straightforward, as it is
 313 influenced by weak layer properties (specific fracture energy), slab properties (e.g. layering), and test geometry.

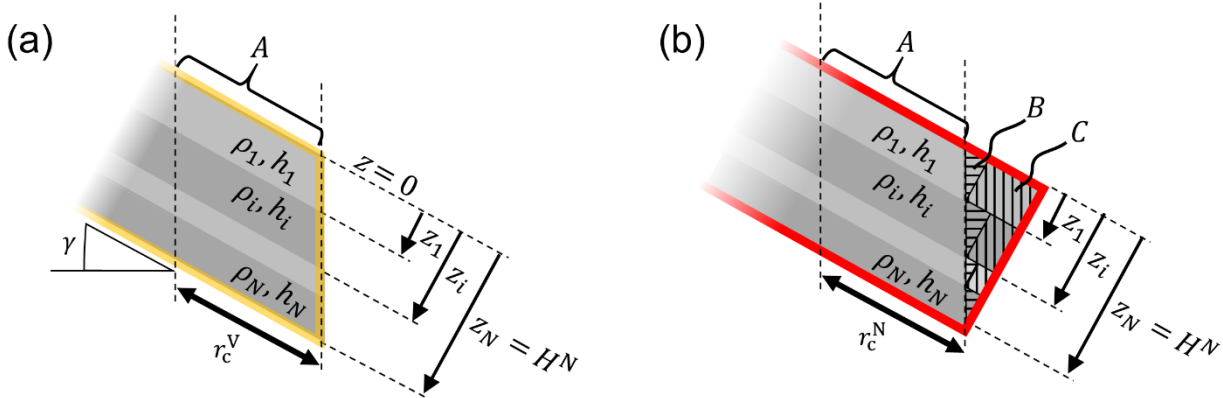
314
 315 Based on our findings, we show that PSTs with slope normal ends and a saw cut in upslope direction (Figure 1a) lead to
 316 the shortest critical cut lengths. Hence, this procedure gives us the most conservative information on crack propagation
 317 propensity (without post-processing). In addition, shorter critical cut lengths ensure that the overall column length is less
 318 likely to influence test result. However, the disadvantage of this approach is the greater effects of slope angle on critical
 319 cut lengths than for vertically cut PSTs. In order to compare tests on different slopes, this effect must be compensated for,
 320 which is not yet straight forward. For an unbiased interpretation of PST results, experiments therefore need to be post-
 321 processed before results from different snow packs, slope inclinations, etc. are compared or combined.
 322 ~~However, if the PST is to be used as a stability tool without further investigation, the vertical PST configuration should~~
 323 ~~be preferred by practitioners as it allows results to be extrapolated from flatter terrain to steeper slopes with less error.~~

324
 325 In general, the use of consistent PST standards will ensure that PST results are easy to interpret, will ensure scientific
 326 rigor and will improve the comparability of tests and their results. In addition, standardization and conversion models
 327 facilitate the comparison of results between researchers, leading to a deeper understanding of snowpack behavior. Prac-
 328 titioners also benefit from standardized methods and interpretation aids that are invaluable in assessing avalanche risk
 329 based on stability tests.

330
 331 **Appendix A:**

332 The load above the saw cut of a PST with slope vertical geometry (V-PST) is independent of the slope angle. However,
 333 the load of a PST with slope normal edges (N-PST) is not. In sloped terrain, a N-PST has more load above the saw cut
 334 than a V-PST. The difference depends on the slope angle, but the layering also has an influence. Layers close to the snow
 335 surface contribute more to the extra load than layers close to the weak layer (of the saw cut). In order to express the
 336 relationship between critical cut lengths (r_c^V, r_c^N) the loads of layered snowpacks (m^V, m^N) have to be formulated through
 337 density ρ_i , thickness h_i and the vertical location z_i of the slab layers i (Figure A1).

338



339

340 **Figure A1: (a) Schematic representation of a layered slab in a PST with slope vertical geometry (V-PST). (b) PST with slope**
 341 **normal geometry (N-PST). In both cases, “A” indicates the volume of the slab above the saw cut r_c^x . The mass of volume A**
 342 **depends on column width b (not indicated), on r_c^x as well as the density ρ_i and thickness h_i of the slab layers i . In (b), the load**
 343 **of the N-PST depends additionally on the slope angle as the Volumes B and C increase with increasing angle.**

344 First for the simpler case of a V-PST (Figure A1a) the mass m^V is given by:

$$345 \quad m^V = m_A = r_c^V b \sum_{i=1}^N h_i \rho_i \quad (A1)$$

346 In the N-PST the Volumes B and C also contribute to the overall mass located above the saw cut:

$$347 \quad m^N = m_A + m_B + m_C \quad (A2)$$

348 The expression for the mass of Volume A remains the same as given in Equation A1. Now, however, the critical crack
 349 length r_c^N is relevant instead of r_c^V . -The masses m_B and m_C are given by:

$$350 \quad m_B = \frac{1}{2} h_1^2 \tan(\gamma) b \rho_1 + \frac{1}{2} h_2^2 \tan(\gamma) b \rho_2 + \dots + \frac{1}{2} h_N^2 \tan(\gamma) b \rho_N = \frac{b \tan(\gamma) \sum_{i=1}^N h_i^2 \rho_i}{2} \quad (A3)$$

$$351 \quad m_C = (z_N - z_1) \tan(\gamma) h_1 b \rho_1 + (z_N - z_2) \tan(\gamma) h_2 b \rho_2 + \dots + (z_N - z_N) \tan(\gamma) h_N b \rho_N$$

$$352 \quad = b \tan(\gamma) \sum_{i=1}^N (z_N - z_i) h_i \rho_i \quad (A5)$$

353 Putting this together results in the overall mass of:

$$354 \quad m^N = \tan(\gamma) b r_c^N \sum_{i=1}^N \frac{h_i \rho_i}{\tan(\gamma)} + \frac{h_i^2 \rho_i}{2 r_c^N} + \frac{(z_N - z_i) h_i \rho_i}{r_c^N} \quad (A4)$$

356 Inserting in Equation A1 results in the layered load model providing the relation between the critical cut lengths r_c^V and
 357 r_c^N :

$$359 \quad r_c^V = r_c^N \frac{\tan(\gamma) \sum_{i=1}^N \frac{h_i \rho_i}{\tan(\gamma)} + \frac{h_i^2 \rho_i}{2 r_c^N} + \frac{(z_N - z_i) h_i \rho_i}{r_c^N}}{\sum_{i=1}^N h_i \rho_i}$$

$$360 \quad = \frac{\sum_{i=1}^N r_c^N h_i \rho_i + \frac{\tan(\gamma)}{2} h_i^2 \rho_i + \tan(\gamma) (z_N - z_i) h_i \rho_i}{\sum_{i=1}^N h_i \rho_i} \quad (A5)$$

362 **Appendix B:**

363 The equations derived in appendix A can be used to formulate a model to correct for imprecisely cut PST beam ends. E.g.
 364 the sawing edge of a PST was close to cut slope normal, but with a deviation of angle β from slope normal (or vertical).
 365 As a result, the critical cut length $r_c^{\tilde{N}}$ is measured in such an experiment. To account for this deviation, we have to add a
 366 mass m_D in Equation A2. Note that this “mass” can be negative in the case β is negative (less overhanging mass than the
 367 slope normal cut). The mass m_D has the same contributions as m_B and m_C but is computed from the angle of error β :

$$368 \quad m_D = \frac{b \tan(\beta) \sum_{i=1}^N h_i^2 \rho_i}{2} + b \tan(\beta) \sum_{i=1}^N (z_N - z_i) h_i \rho_i \quad (B1)$$

369 At the end, the loads (Equation 1) provide the relation between the critical cut lengths:

$$m_A(r_c^{\tilde{N}}) + m_B + m_C + m_D = m_A(r_c^N) + m_B + m_C$$

$$\Rightarrow m_A(r_c^N) = m_A(r_c^{\tilde{N}}) + m_D \quad (\text{B2})$$

By inserting the formulations for m_A (equation A1), the formula to correct an imprecisely cut N-PST is derived as:

$$\begin{aligned} r_c^N &= \frac{r_c^{\tilde{N}} b \sum_{i=1}^N h_i \rho_i + b \tan(\beta) \sum_{i=1}^N \frac{h_i^2 \rho_i}{2} + (z_N - z_i) h_i \rho_i}{b \sum_{i=1}^N h_i \rho_i} \\ &= r_c^{\tilde{N}} + \frac{\tan(\beta) \sum_{i=1}^N \frac{h_i^2 \rho_i}{2} + (z_N - z_i) h_i \rho_i}{\sum_{i=1}^N h_i \rho_i} \quad (\text{B3}) \end{aligned}$$

379

Appendix C:

380

381

382

Table C1: Results of 27 pairs of PSTs, critical cut lengths r_c^V and r_c^N indicate whether PST beam ends were cut vertical or slope normal. Slab thickness H^N was measured in slope normal direction. Slope angle is provided in degrees. For further snowpack data we refer to the Appendix D.

PST- pairs	Location Date	Critical cut length r_c^V (cm)	Critical cut length r_c^N (cm)	Slab thickness H^N (cm)	Slope angle (°)
1	Davos 1.12.21	55 (±2)	43 (±2)	62 (±2)	25 (±2)
2	Davos 1.12.21	49 (±2)	36 (±2)	62 (±2)	25 (±2)
3	Davos 1.12.21	47 (±2)	41 (±2)	62 (±2)	25 (±2)
4	Davos 1.12.21	51 (±2)	37 (±2)	62 (±2)	25 (±2)
5	Davos 1.12.21	56 (±2)	46 (±2)	62 (±2)	25 (±2)
6	Davos 1.12.21	61 (±2)	45 (±2)	58 (±2)	25 (±2)
7	Davos 1.12.21	59 (±2)	41 (±2)	58 (±2)	25 (±2)
8	Davos 1.12.21	65 (±2)	47 (±2)	60 (±2)	25 (±2)
9	Davos 1.12.21	66 (±2)	49 (±2)	63 (±2)	25 (±2)
10	Davos 1.12.21	70 (±2)	49 (±2)	63 (±2)	25 (±2)
11	Davos 1.12.21	61 (±2)	42 (±2)	63 (±2)	25 (±2)
12	Davos 1.12.21	63 (±2)	52 (±2)	64 (±2)	25 (±2)
13	Davos 1.12.21	62 (±2)	42 (±2)	64 (±2)	25 (±2)
14	Davos 1.12.21	62 (±2)	49 (±2)	64 (±2)	25 (±2)
15	Davos 1.12.21	67 (±2)	45 (±2)	64 (±2)	25 (±2)
16	Davos 1.12.21	67 (±2)	51 (±2)	67 (±2)	25 (±2)
17	Davos 1.12.21	60 (±2)	45 (±2)	67 (±2)	25 (±2)
18	Bacon Rind 1.20.21	31 (±2)	25 (±2)	57 (±2)	29 (±2)
19	Bacon Rind 1.20.21	33 (±2)	21 (±2)	56 (±2)	30 (±2)
20	Bacon Rind 1.20.21	29 (±2)	16 (±2)	55 (±2)	30 (±2)
21	Bacon Rind 1.20.21	29 (±2)	18 (±2)	55 (±2)	29 (±2)
22	Bacon Rind 1.20.21	23 (±2)	17 (±2)	54 (±2)	29 (±2)
23	Bacon Rind 1.25.21	29 (±2)	15 (±2)	52 (±2)	30 (±2)
24	Bacon Rind 1.25.21	33 (±2)	15 (±2)	53 (±2)	30 (±2)
25	Bacon Rind 1.25.21	30 (±2)	14 (±2)	54 (±2)	30 (±2)
26	Mount Ellis 3.1.21	59 (±2)	38 (±2)	93 (±2)	25 (±2)
27	Mount Ellis 3.1.21	50 (±2)	29 (±2)	95 (±2)	25 (±2)

383

384

385 **Table C2: Critical cut lengths measured at Mount Ellis, Critical cut lengths r_c^{DOWN} and r_c^{UP} indicate if the weak layer was cut**
 386 **downslope or upslope, respectively. Slab thickness H^N was measured in slope normal direction. Slope angle is provided in de-**
 387 **grees. For further snowpack data we refer to the Appendix D.**

388

PST-pairs	Location Date	PST Geometry	Critical cut length r_c^{DOWN} (cm)	Critical cut length r_c^{UP} (cm)	Slab thickness H^N (cm)	Slope angle (°)
1	Bacon Rind 1.25.21	Slope normal	49 (± 2)	15 (± 2)	50 (± 2)	30 (± 2)
2	Bacon Rind 1.25.21	Vertical	24 (± 2)	29 (± 2)	52 (± 2)	30 (± 2)
3	Bacon Rind 1.25.21	Slope normal	29 (± 2)	33(± 2)	54 (± 2)	30 (± 2)
4	Bacon Rind 1.25.21	Vertical	50 (± 2)	50 (± 2)	53 (± 2)	30 (± 2)
5	Bacon Rind 1.25.21	Slope normal	33 (± 2)	14(± 2)	53 (± 2)	30 (± 2)
6	Bacon Rind 1.25.21	Vertical	24 (± 2)	30 (± 2)	53 (± 2)	31 (± 2)

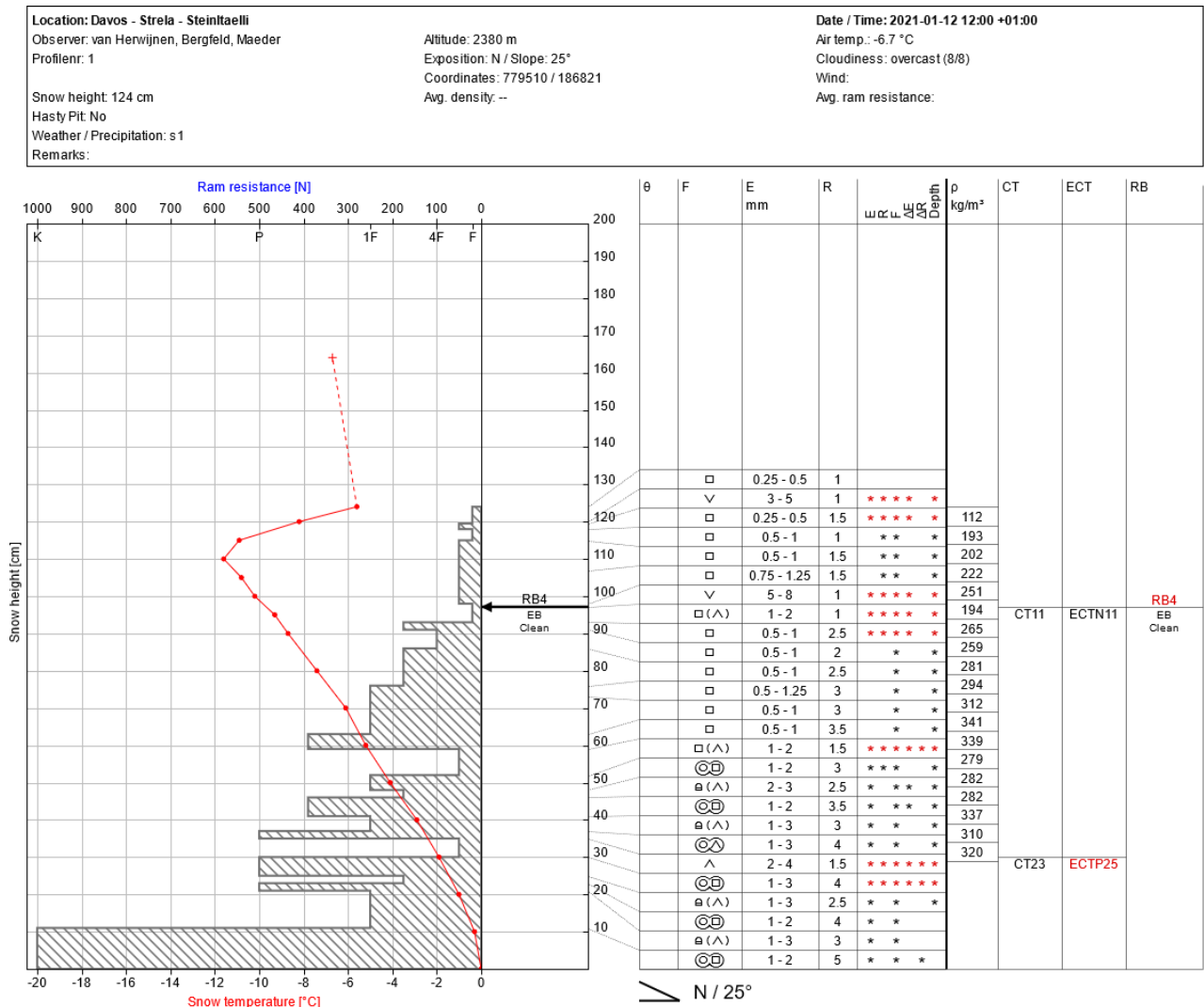
389

390

391 **Appendix D:**

392 At each of our four field sites we took a manual profile including density measures. The following four figures are excerpts
 393 from the corresponding snow profile databanks.

394



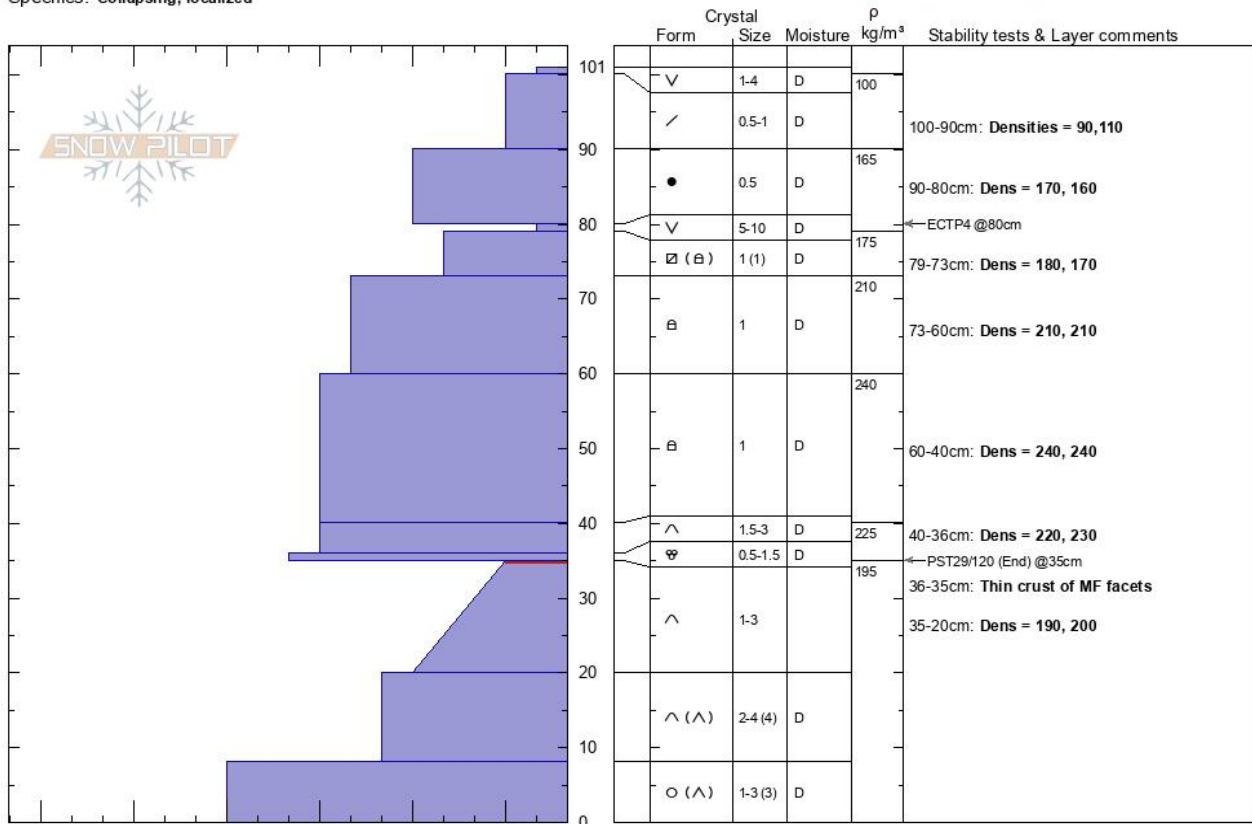
395

396 **Figure D1: Manual profile taken at the Davos field site. The hashed area at the left site represents the hand hardness with snow**
 397 **height, the red line snow temperature with snow height. On the right side, grain type, grain size, hand harness, lemons and**
 398 **snow density are given. On the very right, stability test results are written at the height, of the tested weak layer.**

Bacon Rind Sm Meadow Karl Birkeland
Bridger Range 01/20/2021 - 12:00pm
MT Co-ord: 44.88192N, -111.07457W
 Elevation: 2315 m Slope Angle: 30°
 Aspect: 90° Wind Loading: no
 Specifics: Collapsing, localized

Stability:
 Air Temperature:
 Sky Cover: CLR
 Precipitation: NO
 Wind: Calm

HS: 101 Layer Notes:
 PF: 90 100-90cm: Densities = 90,110
 90-80cm: Dens = 170, 160
 79-73cm: Dens = 180, 170
 73-60cm: Dens = 210, 210
 60-40cm: Dens = 240, 240
 [More Layer Comments below]



Notes: Pit dug to document snow conditions for research on PST geometry.. Additional Layer Comments: 36-40cm: Dens = 220, 230; 35-36cm: Thin crust of MF facets; 20-35cm: Dens = 190, 200; 20-35cm: Problematic layer;

399

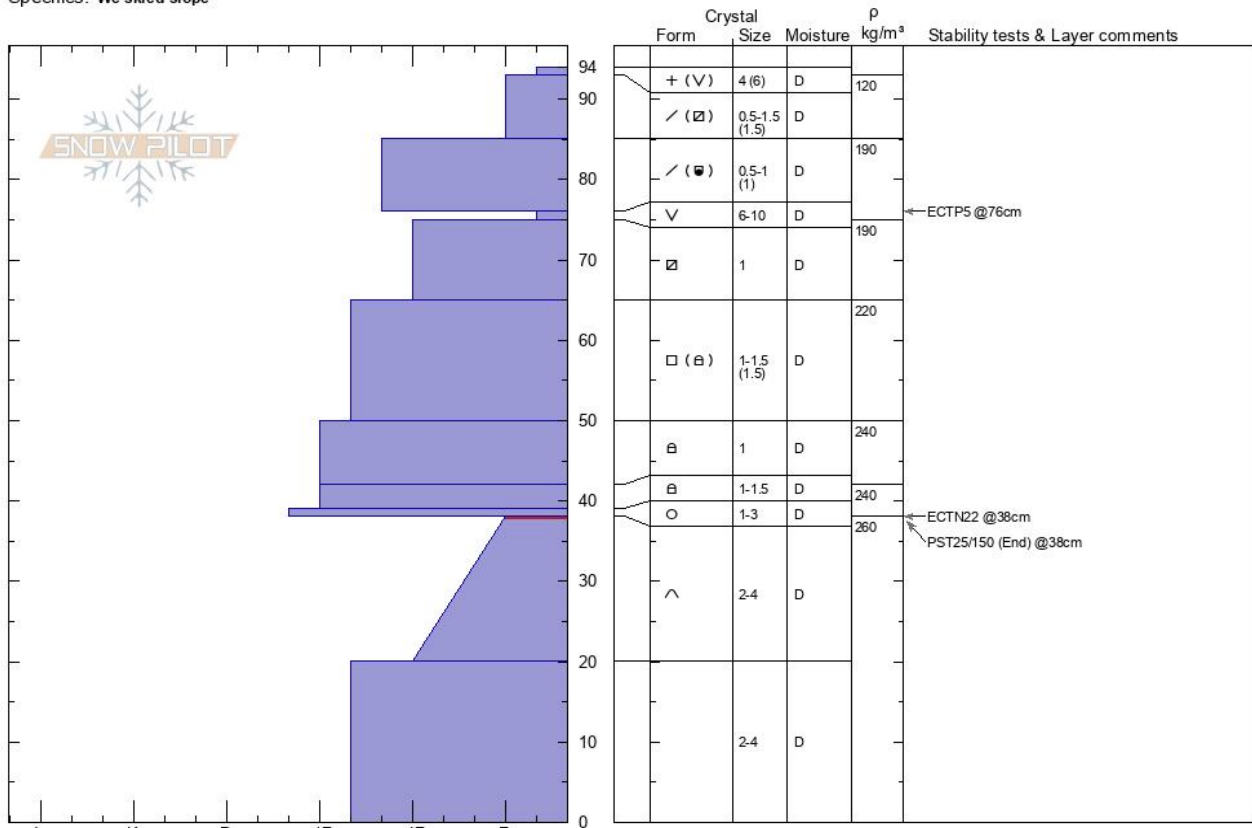
400 **Figure D2: Manual profile taken at the Bacon Rind field site on January 20th 2021. The blue area at the left site represents the**
 401 **hand hardness with snow height, On the right side, grain type, grain size, moisture and snow density are given. On the very**
 402 **right, stability test results are written at the height, of the tested weak layer.**

Bacon Rind Sm Meadow
Madison Range-S
MT
 Elevation: **2321 m**
 Aspect: **80°**
 Specifics: **We skied slope**

Karl Birkeland
01/25/2021 - 12:00pm
 Co-ord: **44.84934N, -111.07942W**
 Slope Angle: **30°**
 Wind Loading:

Stability:
 Air Temperature:
 Sky Cover: **CLR**
 Precipitation: **NO**
 Wind: **Calm**

HS: **94** Layer Notes:
 38-20cm: **Problematic layer**



Notes: Pit dug to document snow conditions for research on PST geometry.

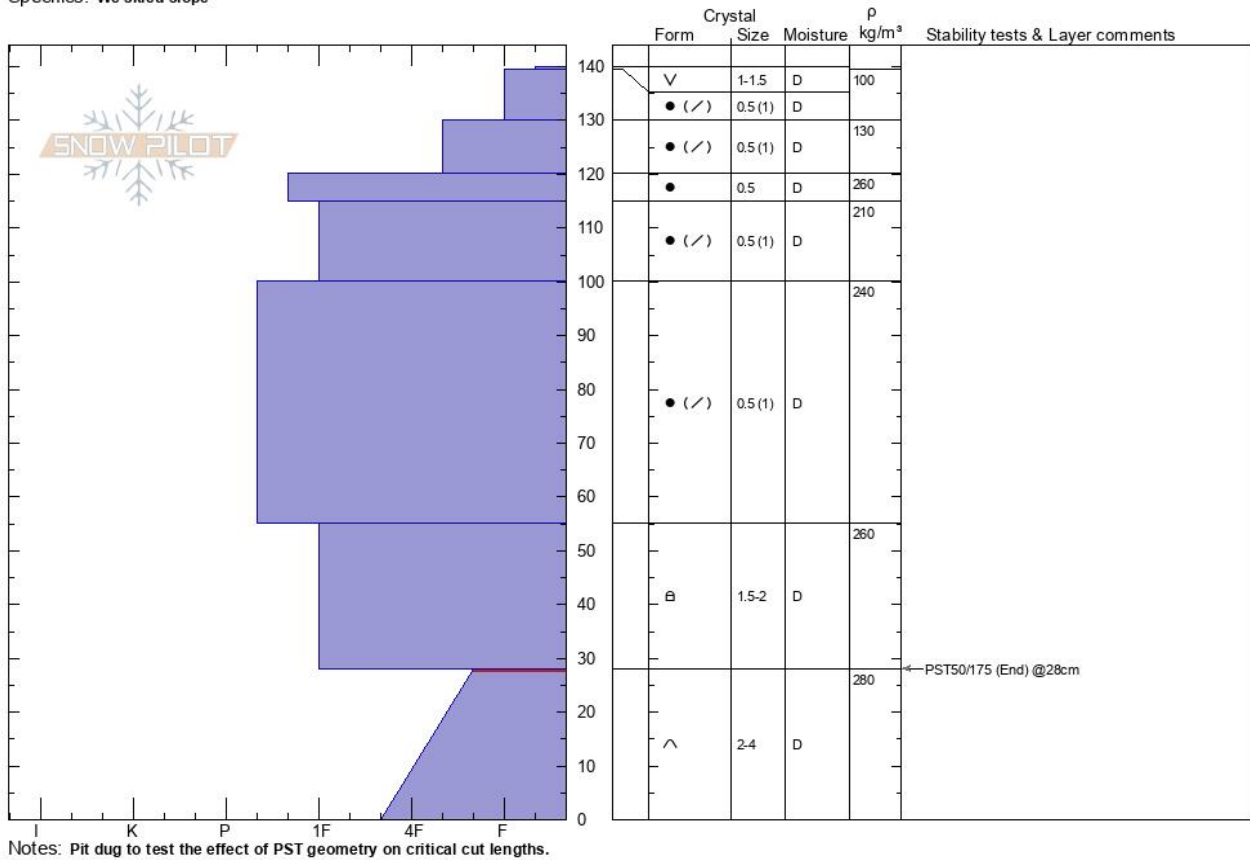
403
 404 **Figure D3: Manual profile taken at the Bacon Rind field site on January 25th. The blue area at the left site represents the hand**
 405 **hardness with snow height, On the right side, grain type, grain size, moisture and snow density are given. On the very right,**
 406 **stability test results are written at the height, of the tested weak layer.**
 407

Mt Ellis
Gallatin Range-N
MT
 Elevation: **2439 m**
 Aspect: **25°**
 Specifics: **We skied slope**

Karl Birkeland
03/01/2021 - 12:00pm
 Co-ord: **45.58173N, -110.95616W**
 Slope Angle: **27°**
 Wind Loading:

Stability:
 Air Temperature:
 Sky Cover: **CLR**
 Precipitation: **NO**
 Wind: **Calm**

HS: 140 Layer Notes:
 28-0cm: **Problematic layer**



408

409 **Figure D4: Manual profile taken at the Mount Ellis field site on January 25th. The blue area at the left site represents the hand**
 410 **hardness with snow height, On the right side, grain type, grain size, moisture and snow density are given. On the very right,**
 411 **stability test results are written at the height, of the tested weak layer.**

412

413 **Competing interests**

414 The contact author has declared that none of the authors has any competing interests

415 **Acknowledgement**

416 We would like to thank Flavia Maeder, Erika Birkeland, and Alex Marienthal for assisting in the field. This research was
 417 partly supported by the Swiss National Science Foundation (grant no. 200021_169424) and funded by the Deutsche For-
 418 schungsgemeinschaft (DFG, German Research Foundation) under grant no. 460195514.

- 420 Bair, E.H., Simenhois, R., van Herwijnen, A. and Birkeland, K., 2014. The influence of edge effects on crack propagation in snow stability
421 tests. *The Cryosphere*, 8(4): 1407-1418.
- 422 Bair, E.H., Simenhois, R., van Herwijnen, A. and Birkeland, K.W., 2013. Edge effects in propagation tests. In: F. Naaim-Bouvet, Y. Durand
423 and R. Lambert (Editors), *Proceedings ISSW 2013. International Snow Science Workshop, Grenoble, France, 7-11 October*
424 *2013. ANENA, IRSTEA, Météo-France, Grenoble, France*, pp. 335-356.
- 425 Bergfeld, B., van Herwijnen, A., Bobillier, G., Larose, E., Moreau, L., Trotter, B., Gaume, J., Cathomen, J., Dual, J. and Schweizer, J.,
426 2022. Crack propagation speeds in weak snowpack layers. *Journal of Glaciology*, 68(269): 557-570.
- 427 Bergfeld, B., van Herwijnen, A., Bobillier, G., Rosendahl, P.L., Weißgraeber, P., Adam, V., Dual, J. and Schweizer, J., 2023. Temporal
428 evolution of crack propagation characteristics in a weak snowpack layer: conditions of crack arrest and sustained propagation.
429 *Natural Hazards and Earth System Sciences*, 23(1): 293-315.
- 430 Bergfeld, B., van Herwijnen, A., Reuter, B., Bobillier, G., Dual, J. and Schweizer, J., 2021. Dynamic crack propagation in weak snowpack
431 layers: insights from high-resolution, high-speed photography. *The Cryosphere*, 15(7): 3539-3553.
- 432 Birkeland, K.W., van Herwijnen, A., Reuter, B. and Bergfeld, B., 2019. Temporal changes in the mechanical properties of snow related to
433 crack propagation after loading. *Cold Regions Science and Technology*, 159: 142-152.
- 434 CAA, 2016. *Technical Aspects of Snow Avalanche Risk Management—Resources and Guidelines for Avalanche Practitioners in Canada*,
435 *Canadian Avalanche Association, Revelstoke, BC, Canada*.
- 436 Fierz, C., Armstrong, R.L., Durand, Y., Etchevers, P., Greene, E., McClung, D., Nishimura, K., Satyawali, P.K. and Sokratov, S., 2008.
437 The 2008 international classification of seasonal snow on the ground. In: C. Campbell, S. Conger and P. Haegeli (Editors),
438 *Proceedings ISSW 2008, International Snow Science Workshop, Whistler, Canada, 21-27 September 2008*, pp. 579-580.
- 439 Gaume, J., van Herwijnen, A., Chambon, G., Wever, N. and Schweizer, J., 2017. Snow fracture in relation to slab avalanche release:
440 critical state for the onset of crack propagation. *The Cryosphere*, 11(1): 217-228.
- 441 Gauthier, D. and Jamieson, B., 2008a. Evaluation of a prototype field test for fracture and failure propagation propensity in weak snowpack
442 layers. *Cold Regions Science and Technology*, 51(2-3): 87-97.
- 443 Gauthier, D. and Jamieson, B., 2008b. Fracture propagation propensity in relation to snow slab avalanche release: Validating the
444 Propagation Saw Test. *Geophysical Research Letters*, 35(13): L13501.
- 445 Gauthier, D. and Jamieson, J.B., 2006a. Evaluating a prototype field test for weak layer fracture and failure propagation. In: J.A. Gleason
446 (Editor), *Proceedings ISSW 2006. International Snow Science Workshop, Telluride CO, U.S.A., 1-6 October 2006*, pp. 107-116.
- 447 Gauthier, D. and Jamieson, J.B., 2006b. Towards a field test for fracture propagation propensity in weak snowpack layers. *Journal of*
448 *Glaciology*, 52(176): 164-168.
- 449 Greene, E., Birkeland, K.W., Elder, K., McCammon, I., Staples, M., Sharaf, D., Trautman, S. and Wagner, W., 2022. *Snow, Weather, and*
450 *Avalanches: Observation Guidelines for Avalanche Programs in the United States. American Avalanche Association, Denver*
451 *CO, U.S.A.*, 110 pp.
- 452 Heierli, J., Gumbsch, P. and Zaiser, M., 2008. Anticrack nucleation as triggering mechanism for snow slab avalanches. *Science*,
453 321(5886): 240-243.
- 454 Jamieson, J.B. and Johnston, C.D., 1998. Refinements to the stability index for skier-triggered dry slab avalanches. *Annals of Glaciology*,
455 26: 296-302.
- 456 McClung, D.M., 2009. Dry snow slab quasi-brittle fracture initiation and verification from field tests. *Journal of Geophysical Research-*
457 *Earth Surface*, 114: F01022.
- 458 Morin, S., Horton, S., Techel, F., Bavay, M., Coléou, C., Fierz, C., Gobiet, A., Hagenmuller, P., Lafaysse, M., Ližar, M., Mitterer, C., Monti,
459 F., Müller, K., Olefs, M., Snook, J.S., van Herwijnen, A. and Vionnet, V., 2020. Application of physical snowpack models in
460 support of operational avalanche hazard forecasting: A status report on current implementations and prospects for the future.
461 *Cold Regions Science and Technology*, 170: 102910.
- 462 Richter, B., Schweizer, J., Rotach, M.W. and van Herwijnen, A., 2019. Validating modeled critical crack length for crack propagation in
463 the snow cover model SNOWPACK. *The Cryosphere*, 13(12): 3353-3366.
- 464 Rosendahl, P.L. and Weissgraeber, P., 2020. Modeling snow slab avalanches caused by weak-layer failure - Part 1: Slabs on compliant
465 and collapsible weak layers. *The Cryosphere*, 14(1): 115-130.
- 466 Schweizer, J., Reuter, B., van Herwijnen, A. and Gaume, J., 2016. Avalanche release 101. In: E. Greene (Editor), *Proceedings ISSW*
467 *2016. International Snow Science Workshop, Breckenridge CO, U.S.A., 3-7 October 2016*, pp. 1-11.
- 468 Sigrist, C. and Schweizer, J., 2007. Critical energy release rates of weak snowpack layers determined in field experiments. *Geophysical*
469 *Research Letters*, 34(3): L03502.
- 470 Simenhois, R. and Birkeland, K.W., 2008. The effect of changing slab thickness on fracture propagation. In: C. Campbell, S. Conger and
471 P. Haegeli (Editors), *Proceedings ISSW 2008, International Snow Science Workshop, Whistler, Canada, 21-27 September*
472 *2008*, pp. 755-760.
- 473 van Herwijnen, A., Gaume, J., Bair, E.H., Reuter, B., Birkeland, K.W. and Schweizer, J., 2016. Estimating the effective elastic modulus
474 and specific fracture energy of snowpack layers from field experiments. *Journal of Glaciology*, 62(236): 997-1007.
- 475 Weißgraeber, P. and Rosendahl, P.L., 2023. A closed-form model for layered snow slabs. *The Cryosphere*, 17(4): 1475-1496.